

Geometry-controlled Failure Mechanisms of Amorphous Solids on the Nanoscale

Kallol Paul¹, Ratul Dasgupta², Jürgen Horbach³, and Smarajit Karmakar^{1*}

¹ *TIFR Center for Interdisciplinary Science, Tata Institute of Fundamental Research, 36/P Gopanpally Village, Serilingampally Mandal, RR District, Hyderabad, 500075, Telangana, India,*

² *Department of Chemical Engineering, IIT Bombay, Powai, Mumbai 400076, India,*

³ *Institute für Theoretische Physik II, Heinrich-Heine-Universität Düsseldorf, 40225 Düsseldorf, Germany*

Amorphous solids, confined on the nano-scale, exhibit a wealth of novel phenomena yet to be explored. In particular, the response of such solids to a mechanical load is not well understood and, as has been demonstrated experimentally, it differs strongly from bulk samples made of the same materials. Failure patterns and mechanisms are strongly affected by the geometry of the confinement and the interplay between interfacial effects in the sample and the time scale, imposed by an external mechanical field. Here, we present the mechanism of cavity formation in a confined model glass, subjected to expansion with a constant strain rate. This system is studied for varying geometric aspect ratio and sample size. Our results show that for a given temperature and straining condition, the sample shows cavitation when the aspect ratio reaches a critical value and below this aspect ratio the sample breaks by forming a neck. The critical aspect ratio is associated with a critical curvature of the neck that depends on strain rate and temperature. If this critical curvature is exceeded, the free energy of the system is minimized by the formation of a cavity. Our study reveals a novel mechanism of cavity formation on the nanoscale. This is probably a generic mechanism for material's failure in small confined systems under mechanical load.

INTRODUCTION

Understanding the failure mechanisms of amorphous solids under external loading is one of the most active research fields amongst scientific as well as engineering community [1–14]. This is mainly due to its importance in fundamental science and industrial applications [10, 15]. It is experimentally known that amorphous solids have much larger failure strength than their crystalline counterpart with similar compositions, but amorphous solids show catastrophic failure which severely limits their applicability as a useful design material [9, 13, 16–20]. Bulk materials that show catastrophic failure by forming cracks under applied load are generically termed as brittle materials [17, 21–23]. On the other hand, some materials show significant plastic deformation before final failure and they are called ductile materials [24, 25]. In Fig. 1, we show representative failure morphology for brittleness and ductility for small systems on the nanoscale. For brittle failure (top panel) the rough failure surface is noticeable while for ductile failure (bottom panel), the neck formation is very prominent. Reducing brittleness of strongly confined amorphous solids is of considerable practical importance.

Recent studies [26–31] suggest that the nature of plasticity in materials depends very significantly on their size. It has been demonstrated experimentally that failure patterns and mechanisms in nano-scale systems can be very different from those of bulk samples of the same materials. Typically, a bulk metallic glass can sustain only up to 2% strain before failing via brittle crack formation. However, uniaxial strain experiments, performed in Ref. [28] on metallic glasses with different sample sizes, show that the strain before failure can increase up to

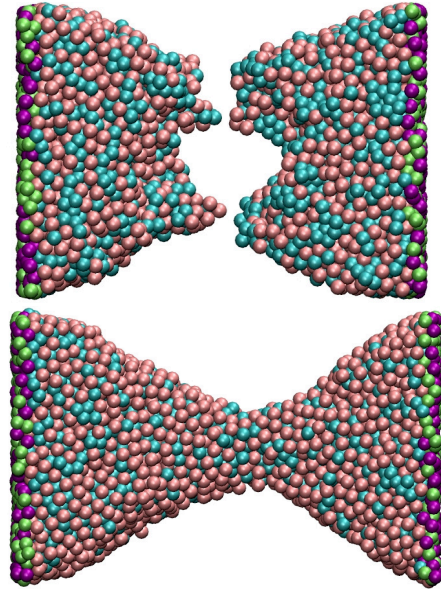


FIG. 1. Morphologies of Brittle and Ductile failures in model glass forming liquids.

200% when the sample size is reduced to 100nm. For such nano-sized sample, it has been also found that the sample may break via the formation of necks. These necks can shrink to chain-like structures as thin as a few atomic layers. This necking in nano-scale samples also indicate a ductile rather than a brittle behaviour of the material in response to deformation.

The change of the mechanical response with reducing sample size has been also observed in uniaxial compression experiments. In Ref. [26], such experiments on

pillers made of metallic glasses are presented. Here, it is shown that pillers with diameters larger than 100 nm show prominent shear band formation, a hallmark of brittle failure. However, pillers that are less than 100 nm in diameter display homogeneous plastic deformation without shear localization. Similarly, Greer *et al.* [29] have demonstrated that size reduction affects the brittle-to-ductile transition in metallic glasses. They have also indicated that the brittle-to-ductile transition is associated with a critical size. Several experiments and simulations of metallic glasses confirm that size reduction increases the material ductility due to surface states [27, 28]. Thus, it is clear that plasticity and failure mechanisms for a material can change very significantly with the physical size and dimension of the sample. A microscopic understanding of these observations would be very important for the systematic development of nano-materials with specific mechanical properties.

The goal of the present study is to understand the nature of plasticity when the system size is reduced from bulk to nano-scale and also to find out the microscopic origin of the observed differences. We have performed uniaxial elongation simulations of a model glass in nano-confinement in order to understand the effects of small sample size on the failure mechanisms and investigate the controlling parameters that determine whether a material will fail via neck formation or via the formation of cavities.

RESULTS

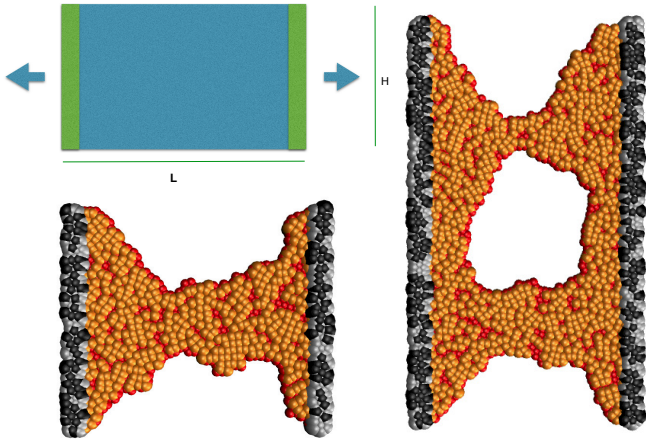


FIG. 2. Top left panel: Schematic of extensional simulation. Bottom left panel: Representative example of failure of a sample via neck formation. Right panel: Similar representative example of failure of a sample via cavity formation.

We have performed numerical simulations in which we chose a model glass former (see Supplementary Material

(SM) for further details of the model) and prepared an amorphous solid by cooling the supercooled liquid at a certain cooling rate (see the method section for details). Then, we put a uniaxial load on it until the material breaks completely. In all these systems the numerical experiments are designed as follows. We first equilibrate the model liquids at some high temperature and then cool it to a low temperature below the experimental glass transition temperature defined as the temperature where the relaxation time reaches a value of 10^6 . Then, at that low temperature, we put a barostat and perform constant pressure and temperature (NPT) simulations at zero pressure such that one can remove the periodic boundary condition. We now define two side walls at the two ends of the solid in the x -direction by freezing the motion of the particles in the two end regions as depicted in the cartoon in Fig. 2.

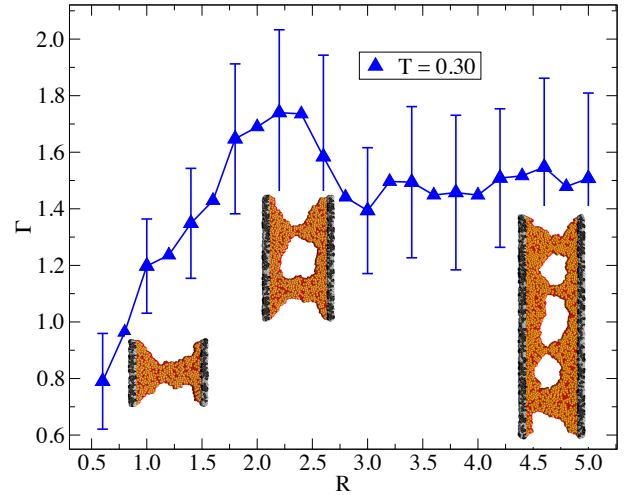


FIG. 3. Variation of maximum strain, Γ , with increasing aspect ratio, R at $T = 0.30$ and $\dot{\gamma} = 5 \times 10^{-6}$. The cross over in failure mechanism is also shown by plotting the morphologies of the samples before the complete failure.

The typical size of this wall is around three inter-particle diameters. The other boundaries are made free. Next, the walls are moved by an increment equal in size and opposite in sign, i.e., the system is subjected to uniaxial strain. To quantify the maximum deformation that a system can withstand before the failure, we have defined the maximum strain as

$$\Gamma = \frac{(L_f - L_0)}{L_0}, \quad (1)$$

where L_0 is the initial (before pulling) length of the system along the tension direction (x direction) and L_f is the final length when the system breaks into two parts. We repeat this numerical simulation for different aspect ratio $R = H/L_0$ ranging from 0.6 to 5.0. H is the width of the system as shown in the schematic diagram in Fig. 2.

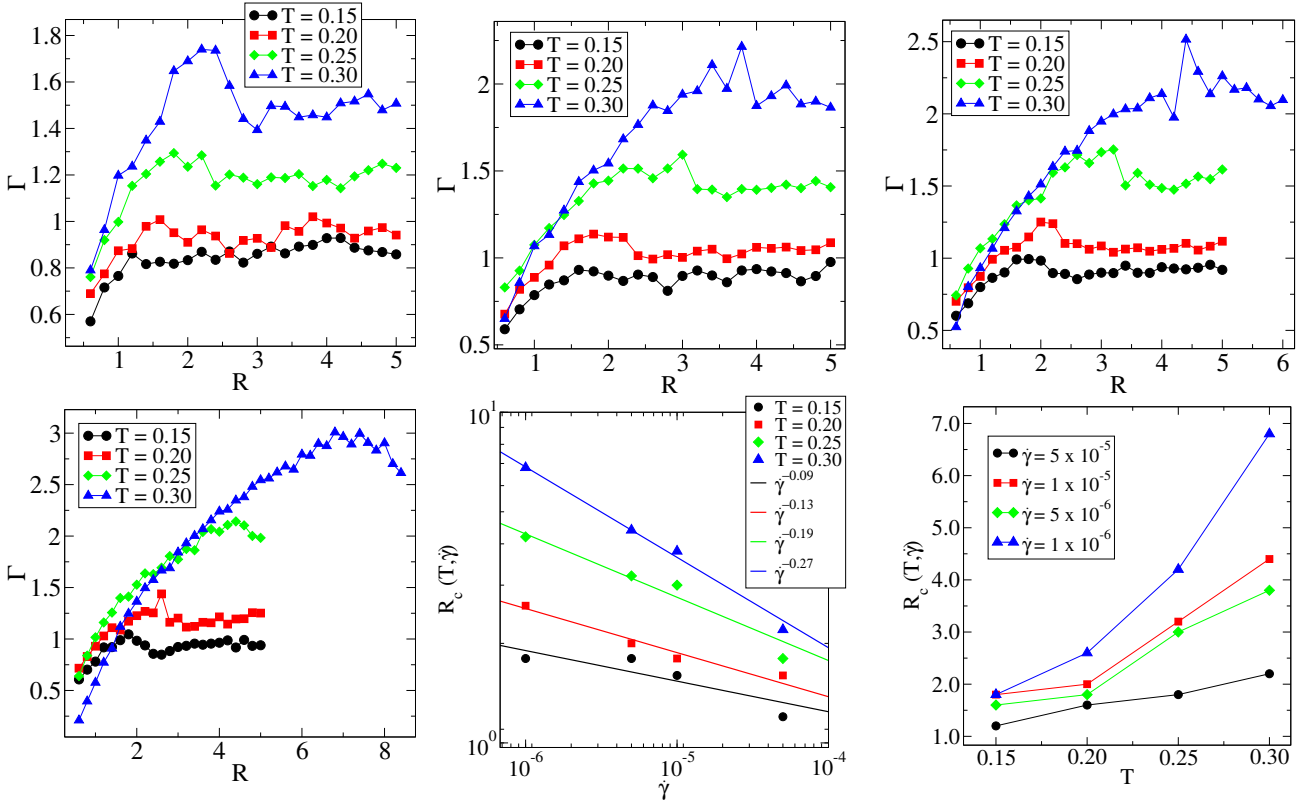


FIG. 4. Variation of maximum strain, Γ as a function of aspect ratio $R = H/L$ for different temperature T at strain rate $\dot{\gamma} = 5 \times 10^{-5}$ (top-left), 10^{-5} (top-middle), 5×10^{-6} (top-right), and 10^{-6} (bottom-left). Variation of critical aspect ratio, R_c as function of strain rate (bottom middle) and temperature (bottom right) (see text for details).

We have done extensional simulations for different strain rates and temperatures keeping $L_0 = 30.0$ for all the systems with different aspect ratio, R .

In Fig. 3, we have plotted the maximum deformation Γ as a function of aspect ratio, R , for $T = 0.30$ at a strain rate $\dot{\gamma} = 5 \times 10^{-6}$. The observation that as one decreases size of the sample (aspect ratio in this case) the system starts to show significant change in ductility is in complete agreement with the experimental results reported in Refs. [26–29]. The change in maximum strain is around 40% with decreasing aspect ratio at this strain rate. One expects this variation to become even larger at strain rates that are small and comparable to experimental strain rates [32]. As discussed in the subsequent paragraphs, the variation indeed becomes larger with decreasing strain rate. Even more surprising results that need experimental validation is the existence of a critical aspect ratio, R_c , below which one no longer sees an increase in maximum strain, Γ . Γ actually starts to decrease very rapidly with decreasing aspect ratio below this critical aspect ratio, R_c . Thus, the Γ vs. R curve shows a peak which signifies the existence of a favoured geometric aspect ratio at which the material will show maximum ductility.

Next, we try to characterize the failure patterns as one increases the aspect ratio, to elucidate the reason for the existence of a critical aspect ratio and a maximum ductility. As shown in Fig. 3, we found that at very small aspect ratio, $R < R_c$, the system always breaks via neck formation and the failure mechanisms changes very sharply at the critical aspect ratio at which one observes the appearance of a single cavity. With further loading, the cavity increases in size and eventually the cavity becomes large enough that the system breaks into two fragments. As one further increases the aspect ratio, the number of cavities increases by an integer number and one observes the appearance of multiple cavities. At these aspect ratios, the system eventually fails by the merger of cavities into a larger cavity in complete agreement with experimental observations [24, 33–37]. The appearance of cavities above a critical aspect ratio indicates a ductile-to-brittle transition in the material with increasing system size. It has been suggested that the change from brittle to ductile behavior with decreasing system size is related to the enhanced relaxation on the surface layer [7, 8, 21, 27, 29, 38]. To further understand this phenomenon and the effect of surface-induced relaxation, we have done similar uniaxial elongation sim-

ulations at different strain rate and temperature.

Effect of strain rate $\dot{\gamma}$ and temperature T

In Fig. 4, we show the maximum strain, Γ , as a function of the aspect ratio for different temperatures at a given strain rate. The critical aspect ratio R_c increases with increasing temperature and the variation of R_c with temperature is larger as one decreases the strain rate, $\dot{\gamma}$. As shown in Fig. 4, the critical aspect ratio changes from $R_c = 1.2$ to 2.2 for strain rate $\dot{\gamma} = 5 \times 10^{-5}$ (top left panel) as the temperature increases from $T = 0.15$ to 0.30, while with slower strain rate $\dot{\gamma} = 10^{-6}$ the value of R_c increases from 1.8 to around 6.8 in the same temperature range. In the bottom middle panel of Fig. 4, the critical aspect ratio, $R_c(T, \dot{\gamma})$, is plotted as a function of $\dot{\gamma}$ for different temperatures. The critical aspect ratio as a function of strain rate can be described by a power law, $R_c(T, \dot{\gamma}) \sim \dot{\gamma}^\eta$, with exponent η varying strongly with temperature. At low temperature, η is very small and approximately close -0.1 and becomes substantially larger as the temperature is increased towards T_G , the calorimetric glass transition temperature for the model. So at $T = 0.30$, the exponent $\eta \sim -0.27$ is obtained. In the bottom right panel of the same figure, the critical aspect ratio is plotted as a function of temperature for different strain rates. One clearly sees that the critical aspect ratio where failure happens via cavity formation increases to larger values, suggesting the expected behaviour of increased ductility with increasing temperature. This behaviour becomes very strong as one decreases the strain rate and thus, under experimental conditions with very slow straining, one can expect a very strong dependence of the mechanical response on temperature.

Effect of system size

An increasing aspect ratio while keeping L_0 fixed is associated with an increasing system size. It is not obvious whether the cavity formation with increasing aspect ratio is solely a geometric effect. To clarify this issue, we have done simulations with a larger system size ($N = 10000$) at $R = 1.8$ (smaller than $R_C = 2.0$), $T = 0.2$ and $\dot{\gamma} = 10^{-5}$, and monitored the failure mechanisms systematically. We also did another simulation with $N = 500$ at $R = 3.0$ (bigger than R_C). We found that the failure mechanisms for $R < R_C$ remain neck-like even for larger systems. For $R > R_C$, it is cavity-dominated even for smaller system size. Within the studied system size, failure mechanisms seem to be geometric rather than being a system size effect. Although it can be easily argued that at system sizes much larger than the one studied in this work, one will eventually reach the bulk behaviour where the aspect ratio will no longer play any role and

the material will behave like a brittle material. It will be interesting to find out the crossover system size where one obtains this behaviour but that system size is expected to be very large and is beyond the scope of this work.

Coalescence of cavities as a generic mechanism for brittle failure:

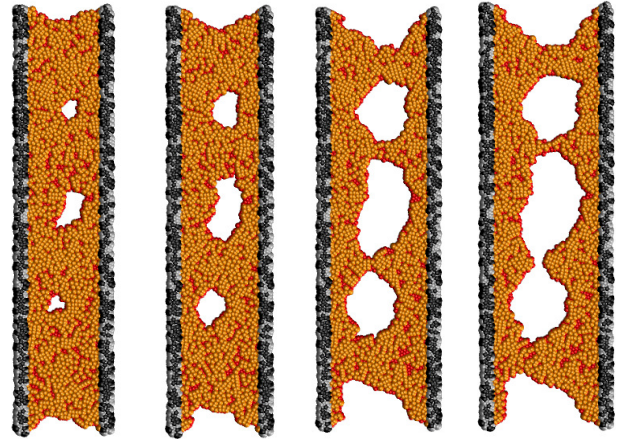


FIG. 5. The appearance and coalescence of multiple cavities for a system with aspect ratio ($R = 4.0$) larger than the critical aspect ratio at $T = 0.20$ and strain rate $\dot{\gamma} = 1 \times 10^{-5}$. Multiple cavities that are spaced almost equal distance from each other first appear in the system and then grow with further uniaxial loading. The cavities then merge to become a large but elongated cavity before pinching the open boundaries. The rough contour of the fracture surface can also be seen.

We now focus on the microscopic failure mechanisms for systems with an aspect ratio much larger than the critical aspect ratio at a given temperature and strain rate. For systems with an aspect ratio larger but close to R_C , a single cavity appears in the middle of the system with increasing deformation and then the cavity increases in size until it meets the open surface to break apart. With further increase in aspect ratio, one observes the appearance of two and then three cavities and this continues with increasing aspect ratio. One also observes that the cavities generally appear at equal distance from each other and if the straining is stopped and the cavities are allowed to relax, they remain at that size without closing them. This indicates that the cavities formed during straining are very stable at least in the studied time duration. For aspect ratios at which multiple cavities are formed during straining, first cavities coalesce to become a large single cavity with further deformation and then finally meets the open boundary. In Fig. 5, we have shown such a process of cavity merger for a system with an aspect ratio $R = 4.0$ at $T = 0.20$ and $\dot{\gamma} = 1 \times 10^{-5}$.

One can clearly see that the first three cavities form in the middle of the sample almost equally spaced. Then, these cavities become larger in size maintaining roughly their separation. Finally, they merge to become a larger but elongated cavity before pinching off the open boundaries. Coalescence of multiple cavities is found to be a very generic mechanism for failure in these systems with a larger aspect ratio. This implies that for bulk brittle materials failure happens generically via formation and coalescence of cavities. As for a given aspect ratio, certain numbers of cavities form and then merge, one should be able to understand the morphology and roughness of the brittle crack surface from the typical size of these cavities before their merger. In the rightmost panel of Fig. 5, one can also see the rough fracture contour which has a scale roughly equal to the radius of the cavities before the merger. A much detailed systematic analysis on a larger system size is needed to have some understanding on this.

Results from 3D systems:

Until now, results for amorphous solids in two dimensions have been presented. A natural question is to see to what extent these results also hold in three dimensional systems. Our initial results of uniaxial elongation tests for three-dimensional samples under similar loading conditions and temperatures indeed suggest that the change in failure mechanism from necking to cavity formation with changing aspect ratio is also seen in three dimensional systems (see SI for further details). So it seems that the existence of a critical aspect ratio above which cavity formation dominates the failure mechanism under uniaxial elongation is a generic phenomenon and does not depend on the dimensionality of the sample. It will also be very interesting to understand the failure in three-dimensional nano-sized systems by varying systematically the cross-sectional area of the sample from square to rectangular to circular. If one of the side are made much smaller than another side, one will have a system which will be quasi two dimensional or like a thin film and failure mechanisms with increasing film thickness might be important and interesting for practical applications.

Curvature of the open surface

To understand the origin of the crossover in the failure mechanism from necking to cavitation, we now analyze the curvature of the free surfaces with increasing strain-ing. To this end, we fit the average morphology of the free surfaces to an ellipse and determine the radius of curvature ($\mathcal{K} = a^2/b$) at the centre of the surface (vertex of the minor axis of the ellipse). In Fig. 6, we show a typical snapshot of the surface particles and a fit to it

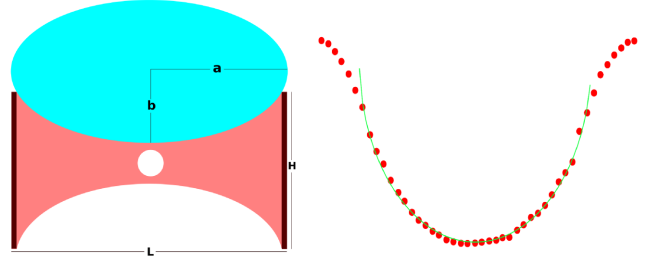


FIG. 6. schematic diagram of a surface fitting with an ellipse

with the equation of an ellipse. As can be inferred from this snapshot, the fitting of the morphology of the free surfaces works very well and therefore the estimate of the curvature is expected to be reliable.

Variation of radius of curvature with aspect ratio

In Fig. 7, we show the curvature of the free boundary at $T = 0.2$ and $\dot{\gamma} = 5 \times 10^{-6}$ for different aspect ratio.

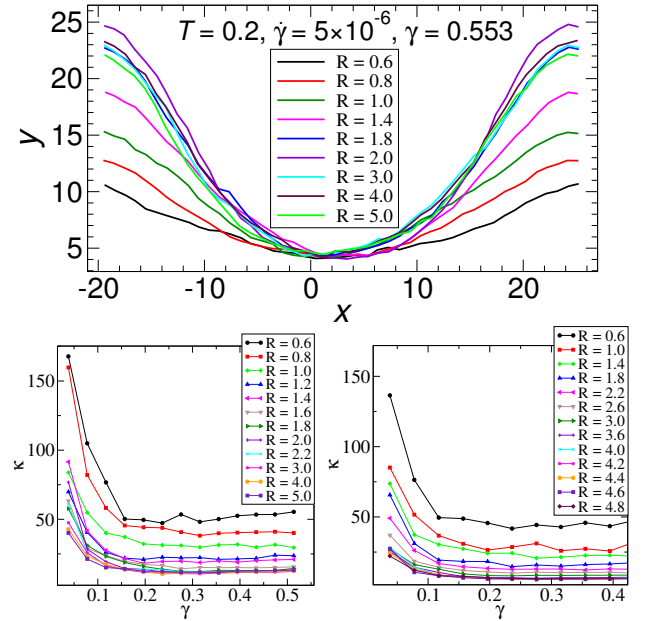


FIG. 7. Radius of curvature at a constant strain for different aspect ratio. Radius of curvature as a function of strain for different aspect ratio at $T = 0.25$ and $\dot{\gamma} = 10^{-5}$ (left), 10^{-6} (right)

It is clear that the radius of curvature (\mathcal{K}) is decreasing down to a certain value as the aspect ratio R is increased. The radius of curvature starts to saturate at $R \simeq 2.0$, which is close to the critical aspect ratio R_c at $T = 0.2$ and $\dot{\gamma} = 5 \times 10^{-6}$. This observation clearly

indicates that once R reaches R_c , the curvature of the surface can no longer increase. Thus the system gets constrained to generate more surface area by increasing the curvature via necking and it leads to cavity formation in the bulk. Fig. 7 shows the evolution of curvature as a function of strain, γ , for different aspect ratios R at a particular temperature $T = 0.25$ and strain rates $\dot{\gamma} = 5 \times 10^{-5}$ (left panel) and 10^{-6} (right panel). The radius of curvature initially decreases monotonically and then reaches a plateau with increasing strain for each aspect ratio. Beyond the critical aspect ratio, the curvature seems to become the same for all aspect ratios. The aspect ratio at which this happens tends to increase with decreasing strain as can be observed from the data shown in the right panel of Fig. 7.

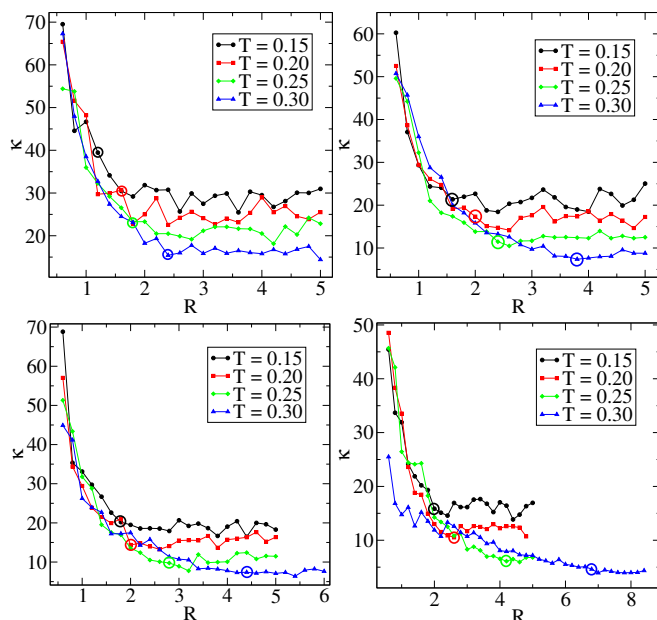


FIG. 8. Radius of curvature as a function of aspect ratio for different temperature and strain rate for different temperature T at strain rate $\dot{\gamma} = 5 \times 10^{-5}$ (top-left), 10^{-5} (top-right), 5×10^{-6} (bottom-left), and 10^{-6} (bottom-right)

In Fig. 8, we show the radius of curvature \mathcal{K} at $\gamma = 0.236$ as a function of the aspect ratio R for different temperatures T and strain rates $\dot{\gamma}$. For all the studied cases, the radius of curvature starts to saturate after values of R that are close to the critical aspect ratio, R_c , at that T and $\dot{\gamma}$. In this figure, we also highlight the value of the corresponding R_c , that we computed earlier from the variation of Γ . The correspondence between the value of R_c at which Γ vs. R has a peak and the value at which \mathcal{K} vs. R reaches a saturation value, is undoubtedly very good (see SI for further details).

CONCLUSIONS

We have performed uniaxial extensile deformation simulations of a model amorphous solids to understand the microscopic origin of cavitation and its connection to ductility in nano-sized amorphous solids. In this work, we have explored some of the main controlling parameters that determine whether the solid will fail via formation of cavities or via necking when subjected to external uniaxial extensional load. Our findings clearly suggest that the aspect ratio of the sample is one of the key parameters that control whether the failure will be via necking or will be dominated by cavity formation. We also showed for the first time that there exists a critical aspect ratio at which the ductility of the material is maximal and the failure mechanism is very different below and above this critical aspect ratio. Our results confirm that all the samples having an aspect ratio below its critical value will fail via necking whereas samples having aspect ratio larger than the critical value always forms cavities inside bulk before it breaks into two segments. Also, the number of cavities increases as one increases the aspect ratio. Our observations also show that this critical aspect ratio is a strong function of temperature and strain rate as the value of critical aspect ratio becomes larger at lower strain rate and higher temperature. Thus the ductility of amorphous solid on the nano-scale depends strongly on temperature and strain rate. Not much system size dependence in the failure mechanism is observed within the studied system size range and it completely depends upon its geometrical aspect ratio. Thus the conventional notion of enhanced relaxation due to surface states leading to an increase in ductility of the material at nano-scale may not be completely correct as geometric parameters also seem to play a big role. We believe that our observation of a crossover between neck-like failure to cavity-dominated failure across a critical aspect ratio will help us in future to understand why formation and subsequent merger of cavities are generic mechanisms for brittle failure on small length scales.

METHOD SECTION

We have studied a generic model binary glass former in two dimensions [39]. The equations of motion are integrated with a leap-frog algorithm, using an integration time step of $\delta t = 0.005 \tau$ with $\tau = \sqrt{m\sigma_{AA}^2/\varepsilon_{AA}}$. The temperature was kept constant via a Berendsen thermostat. The number of particles N varied from 648 to 5400 and the bi-dispersity ratio was 65 : 35 (A : B).

In our simulations, we used a protocol similar to in the recent study by Babu *et al.* [39]: First, we generate 32 independent configurations at the high temperature $T = 1.0$. To this, the end, simulations over 10^6 time steps in the NAT ensemble are performed, applying periodic

boundary conditions (PBC) in the two spatial directions. Then, these configurations are cooled down to a desired temperature in the range $0.15 \leq T \leq 0.3$ with a cooling rate of 0.001, followed in each case by an *NPT* simulation at zero pressure, i.e. $P = 0.0$, for another 2×10^5 steps. Then, we remove the PBC, introducing free boundaries in the y direction and confining the system in x direction by two disordered walls. The two walls are obtained by pinning particles in layers of thickness $3\sigma_{AA}$ on both sides in x direction. Now the system is at the desired temperature and zero pressure, and both walls are uniaxially pulled in the opposite direction with a constant strain rate $\dot{\gamma}$. We vary the strain rate in the range $5 \times 10^{-5} \leq \dot{\gamma} \leq 10^{-6}$. At each strain rate, the system is deformed until it breaks completely into two parts.

We would like to thank Pinaki Chaudhuri, Surajit Sengupta and Srikanth Sastry for useful discussion.

* smarajit@tifrh.res.in

- [1] A. Argon, *Acta Metallurgica* **27**, 47 (1979).
- [2] C. E. Maloney and A. Lemaître, *Physical Review E* **74**, 016118 (2006).
- [3] C. Maloney and A. Lemaître, *Phys. Rev. E* **74**, 016118 (2006).
- [4] H. G. E. Hentschel, S. Karmakar, E. Lerner, and I. Procaccia, *Physical Review Letters* **104**, 025501 (2010).
- [5] S. Karmakar, E. Lerner, I. Procaccia, and J. Zylberg, *Physical Review E* **82**, 031301 (2010).
- [6] S. Karmakar, E. Lerner, and I. Procaccia, *Physical Review E* **82**, 055103 (2010).
- [7] O. Dauchot, S. Karmakar, I. Procaccia, and J. Zylberg, *Phys. Rev. E* **84**, 046105 (2011).
- [8] M. Lagos and R. Das, *Advances in Applied Mathematics and Mechanics* **8**, 485 (2016).
- [9] T. C. Hufnagel, C. A. Schuh, and M. L. Falk, *Acta Materialia* **109**, 375 (2016).
- [10] M. Chen, *Annual Review of Materials Research* **38**, 445 (2008), <https://doi.org/10.1146/annurev.matsci.38.060407.130226>.
- [11] M. Ashby and A. Greer, *Scripta Materialia* **54**, 321 (2006), viewpoint set no: 37. On mechanical behavior of metallic glasses.
- [12] D. Rodney, A. Tanguy, and D. Vandembroucq, *Modelling and Simulation in Materials Science and Engineering* **19**, 083001 (2011).
- [13] C. Schuh, T. Hufnagel, and U. Ramamurty, *Acta Materialia - ACTA MATER* **55**, 4067 (2007).
- [14] G. P. Shrivastav, P. Chaudhuri, and J. Horbach, *Physical Review E* **94**, 042605 (2016).
- [15] A. L. Greer, *Science* **267**, 1947 (1995).
- [16] K. Binder, J. Horbach, W. Kob, and A. Winkler, "Computer simulation of molten and glassy silica and its mixtures with sodium oxide and aluminium oxide," in *Complex Inorganic Solids: Structural, Stability, and Magnetic Properties of Alloys*, edited by P. E. A. Turchi, A. Gonis, K. Rajan, and A. Meike (Springer US, Boston, MA, 2005) pp. 35–53.
- [17] J. Schroers and W. L. Johnson, *Phys. Rev. Lett.* **93**, 255506 (2004).
- [18] B. Schuster, Q. Wei, M. Ervin, S. Hruszkewycz, M. Miller, T. Hufnagel, and K. Ramesh, *Scripta Materialia* **57**, 517 (2007).
- [19] S. Scudino, H. Shakur Shahabi, M. Stoica, I. Kaban, B. Escher, U. Kühn, G. B. M. Vaughan, and J. Eckert, *Applied Physics Letters* **106**, 031903 (2015), <https://doi.org/10.1063/1.4906305>.
- [20] B. Sun and W. Wang, *Progress in Materials Science* **74**, 211 (2015).
- [21] H. Guo, P. F. Yan, Y. B. Wang, J. Tan, Z. F. Zhang, M. L. Sui, and E. Ma, *Nature Materials* **6**, 735 EP (2007).
- [22] J. Crété, P. Longère, and J. Cadou, *Computer Methods in Applied Mechanics and Engineering* **275**, 204 (2014).
- [23] G. C. Li, H. Q. Liu, M. L. Du, Y. S. Hong, and X. Zhang, *Fatigue & Fracture of Engineering Materials & Structures* **15**, 187 (1992), <https://onlinelibrary.wiley.com/doi/pdf/10.1111/j.1460-2695.1992.tb00048.x>.
- [24] I. Singh, R. Narasimhan, and U. Ramamurty, *Phys. Rev. Lett.* **117**, 044302 (2016).
- [25] P. Chaudhuri and J. Horbach, *Phys. Rev. B* **94**, 094203 (2016).
- [26] C. A. Volkert, A. Donohue, and F. Spaepen, *Journal of Applied Physics* **103**, 083539 (2008), <https://doi.org/10.1063/1.2884584>.
- [27] D. Z. Chen, D. Jang, K. M. Guan, Q. An, W. A. Goddard, and J. R. Greer, *Nano Letters* **13**, 4462 (2013).
- [28] J. H. Luo, F. F. Wu, J. Y. Huang, J. Q. Wang, and S. X. Mao, *Phys. Rev. Lett.* **104**, 215503 (2010).
- [29] D. Jang and J. R. Greer, *Nature Materials* **9**, 215 EP (2010).
- [30] J. R. Greer and J. T. M. De Hosson, *Festschrift Vaclav Vitek*, *Progress in Materials Science* **56**, 654 (2011).
- [31] O. Kraft, P. A. Gruber, R. Mönig, and D. Weygand, *Annual Review of Materials Research* **40**, 293 (2010), <https://doi.org/10.1146/annurev-matsci-082908-145409>.
- [32] A. Sergueeva, N. Mara, D. Branagan, and A. Mukherjee, *Scripta Materialia* **50**, 1303 (2004).
- [33] B. Ding, X. Li, X. Zhang, H. Wu, Z. Xu, and H. Gao, *Nano Energy* **18**, 89 (2015).
- [34] R. Maaß, P. Birckigt, C. Borchers, K. Samwer, and C. Volkert, *Acta Materialia* **98**, 94 (2015).
- [35] Q. An, G. Garrett, K. Samwer, Y. Liu, S. V. Zybin, S.-N. Luo, M. D. Demetriou, W. L. Johnson, and W. A. Goddard, *The Journal of Physical Chemistry Letters*, *The Journal of Physical Chemistry Letters* **2**, 1320 (2011).
- [36] P. Murali, T. F. Guo, Y. W. Zhang, R. Narasimhan, Y. Li, and H. J. Gao, *Physical Review Letters* **107**, 215501 (2011).
- [37] P. Guan, S. Lu, M. J. B. Spector, P. K. Valavala, and M. L. Falk, *Physical Review Letters* **110**, 185502 (2013).
- [38] P. S. Steif, *Journal of the Mechanics and Physics of Solids* **31**, 359 (1983).
- [39] J. S. Babu, C. Mondal, S. Sengupta, and S. Karmakar, *Soft Matter* **12**, 1210 (2016).

Geometry-controlled Failure Mechanisms of Amorphous Solids on the Nanoscale : Supplementary Materials

Kallol Paul¹, Ratul Dasgupta², Jürgen Horbach³, and Smarajit Karmakar¹

¹ TIFR Center for Interdisciplinary Science, Tata Institute of Fundamental Research,
36/P Gopanpally Village, Serilingampally Mandal,
RR District, Hyderabad, 500075, Telangana, India

² Department of Chemical Engineering, IIT Bombay, Powai, Mumbai 400076, India,

³ Institute für Theoretische Physik II, Heinrich-Heine-Universität Düsseldorf, 40225 Düsseldorf, Germany

I. MODEL AND SIMULATION DETAILS

The model studied is a generic glass former in two dimensions. It is a binary mixture whose amount of bi-dispersity was chosen to avoid crystallization as well as phase separation. A particle of type α and a particle of type β ($\alpha\beta = \text{AA}, \text{AB}, \text{BB}$), separated by a distance r from each other, interact via a Lennard-Jones potential given by

$$\Phi_{\alpha\beta}(r) = \begin{cases} 4\epsilon_{\alpha\beta} \left[\left(\frac{\sigma_{\alpha\beta}}{r} \right)^{12} - \left(\frac{\sigma_{\alpha\beta}}{r} \right)^6 \right], & \text{if } r \leq r_m \sigma_{\alpha\beta} \\ \epsilon_{\alpha\beta} \left[a \left(\frac{\sigma_{\alpha\beta}}{r} \right)^{12} - b \left(\frac{\sigma_{\alpha\beta}}{r} \right)^6 \right] \\ + \sum_{l=0}^2 C_{2l} \left(\frac{r}{\sigma_{\alpha\beta}} \right)^{2l}, & \text{if } r_m \sigma_{\alpha\beta} \leq r \leq r_c \sigma_{\alpha\beta} \\ 0, & \text{if } r \geq r_c \sigma_{\alpha\beta} \end{cases} \quad (1)$$

where r_m is the length where the potential attains its minimum, and r_c is the cut-off length above which the potential vanishes. The coefficients a , b and C_{2l} are chosen such that the repulsive and attractive parts of the potential are continuous with two continuous derivatives at the potential minimum and the potential goes to zero continuously at r_c with two continuous derivatives as well. The values of the parameters a , b and C_{2l} can be found in Ref. [1].

In this work, energies and lengths are given in units of ϵ_{AA} and σ_{AA} , respectively. The parameters of the potential are $\epsilon_{\text{AB}} = 1.5\epsilon_{\text{AA}}$, $\epsilon_{\text{BB}} = 0.5\epsilon_{\text{AA}}$, $\sigma_{\text{AB}} = 0.8\sigma_{\text{AA}}$, and $\sigma_{\text{BB}} = 0.88\sigma_{\text{AA}}$. The Boltzmann constant as well as mass of the particles are set to unity, $k_B = 1.0$ and $m = 1.0$, respectively. Moreover, we set $r_{c,\alpha\beta} = 2.0\sigma_{\alpha\beta}$ and $r_{m,\alpha\beta} = 2^{1/6}\sigma_{\alpha\beta}$. Note that the values of $r_{c,\alpha\beta}$ were chosen such that at the considered density $\rho = \frac{N}{A} = 1.2\sigma^{-2}$ (with N the particle number and A the area of the system) and temperature range the system is in an intermediate state of brittle-ductile transitions [1].

The equations of motion are integrated with a leap-frog algorithm, using an integration time step of $\delta t = 0.005\tau$ with $\tau = \sqrt{m\sigma_{\text{AA}}^2/\epsilon_{\text{AA}}}$. The temperature was kept constant via a Berendsen thermostat. The number of particles N varied from 648 to 5400 and the bi-dispersity ratio was 65 : 35 (A : B).

II. EFFECT OF SYSTEM SIZE

Since L_0 and the density of the system is constant, increasing the aspect ratio basically means the system size is increased. So one can argue that cross over in the failure mechanisms from necking to cavity dominated with increasing aspect ratio, is a purely a system size effect and it is a probably not a geometric phenomenon. As we have already calculated the critical aspect ratio R_C for a particular temperature and strain rate we performed a set of simulations for different system sizes with a range of R varying below and above R_C and monitored the failure mechanism as well as the morphology of the fractured surface for each case. At least within the studied system sizes, it is very clear that only the aspect ratio controls this observed cross over in the failure mechanism with changing the aspect ratio. We also believe that beyond a large system size where the bulk effect of the system will be much more than the surface effect, the system will eventually behave like a brittle material failing via cavity formation inside the bulk at any aspect ratio of the sample. At low temperature and strain rate, this asymptotic bulk size is expected to be much larger than what we can study in a computer simulation.

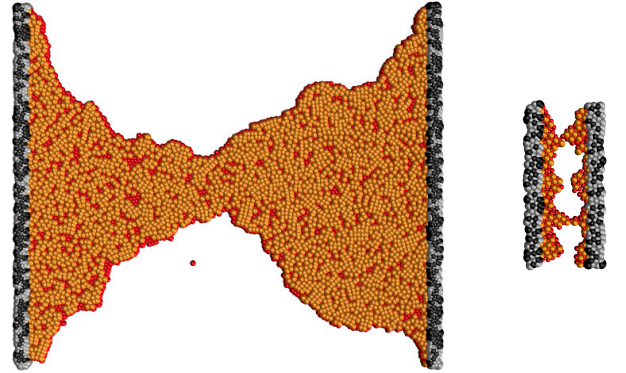


FIG. 1. different failure pattern: (left) $R = 1.6$ $N = 10000$, (right) $R = 3.0$ $N = 500$

In Fig.1, we showed the morphology of two different cases at $T = 0.2$ and strain rate $\dot{\gamma} = 10^{-5}$. In the first case, we chose a relatively large system size $N = 10000$ and aspect ratio $R = 1.8$, which is smaller than R_C at this temperature and strain rate, whereas in the second case

a relatively very small system size $N = 500$ and a larger aspect ratio than R_C , $R = 3.0$ is chosen. The morphology showed that even if in the first case, the system size is large, the failure mechanism is like a ductile material with clear neck formation before the failure, whereas in the other case for a very small system size the failure mechanism is like a brittle material with the formation of a lot of cavities. This observation clearly confirms that at least within the studied system size, it is aspect ratio, not the system size that controls the failure mechanism of these amorphous solids.

III. EFFECT OF INITIALLY INDUCED CAVITY

As we have now some understanding of the existence of critical aspect ratio and its intimate connection to cavity formation, we tried to understand whether the process of cavity formation can be tuned to increase the ductility in these nano-scale samples. We addressed this question by studying the effect of an initial cavity on the failure mechanisms of the system. Our aim is to understand whether there is any possibility to increase the ductility of material through initially inducing cavities. We chose a system with a reasonably larger aspect ratio $R = 4.0$ where three cavities form at a temperature $T = 0.20$ and strain rate $\dot{\gamma} = 1 \times 10^{-5}$. From our earlier simulation results, the maximum ductility of this system is found to be $\Gamma = 1.061$. Now we start with a system in which we remove a segment in the middle of the sample. The thickness of the removed portion is set to twice the potential cut-off length r_c to ensure zero interaction between these two segments.

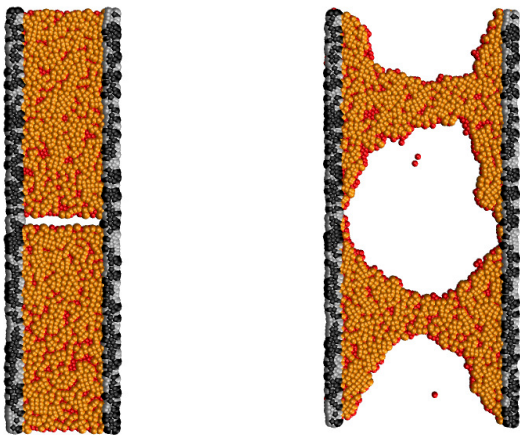


FIG. 2. failing pattern with initial aspect ratio $r = 4.0$ at $T = 0.2$ and $\delta = 10^{-5}$

Under uniaxial elongation, we observed a much a larger cavity appearing in the middle instead of multiple smaller cavities with increasing load as shown in Fig.2. We found that statistically, the system was able to sustain a larger load before failure. The measured value of Γ , in this case,

is found to be around 15% more than the value obtained for the system with no initial cavity. This clearly suggests that an array of nano-pilers are better than bulk materials in terms of their uni-axial load bearing capacity. This observation is again in agreement with recent experimental results where it is suggested that an array of nano-pilers are better candidates for supporting the load at nano-scale.

IV. RESULTS IN THREE DIMENSION

In three dimensions, we can have a variety of geometric shapes, so to make it simpler we have taken a bar geometry in which the length along the elongation axis is kept at L_0 and cross-section of the bar is kept to be square in shape with area equal to $H \times H$. We then varied the cross-section area by increasing H . The aspect ratio is defined similarly as $R = H/L_0$.

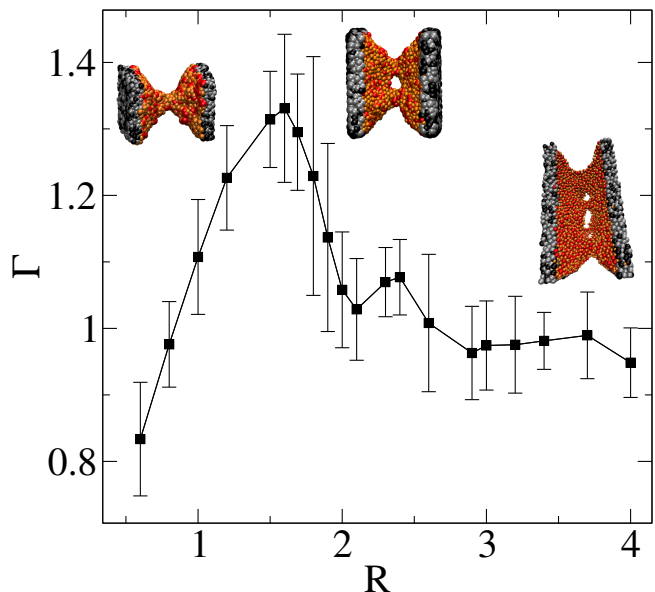


FIG. 3. failing pattern with initial aspect ratio $r = 4.0$ at $T = 0.2$ and $\delta = 10^{-5}$

In Fig.3, we have shown maximum strain Γ for the three dimensional bar type sample at $T = 0.20$ and strain rate $\dot{\gamma} = 1 \times 10^{-5}$. One can clearly see that maximum strain first increases with increasing aspect ratio before reaching a peak at a critical aspect ratio and then decreases quite sharply with further increase in aspect ratio. The results are very similar to the ones obtained for two dimensional systems. The failure mechanisms for systems with aspect ratio smaller than the critical aspect ratio is purely necking and for those with a larger aspect ratio than the critical aspect ratio, failure happens via cavity formation. For much larger aspect ratio, one observes once again the formation of multiple cavities and subsequent merger of them before final failure. Thus we

believe that the existence of a critical aspect ratio above which cavitation plays an important role in determining the failure mechanisms under uni-axial elongation tests are very generic and does not depend on the dimensionality. We believe that it will very interesting to understand the failure mechanisms in these nano-size systems in three dimensions by varying systematically their geometric shapes. For example, if the cross-sectional area is varied from square to rectangular with one of the side being much smaller than another side, one will have a system which will be quasi two dimensional or like a thin film. Failure mechanisms with increasing film thickness will be very important and interesting to understand for practical applications.

V. CURVATURE AT A CONSTANT STRAIN FOR DIFFERENT ASPECT RATIO

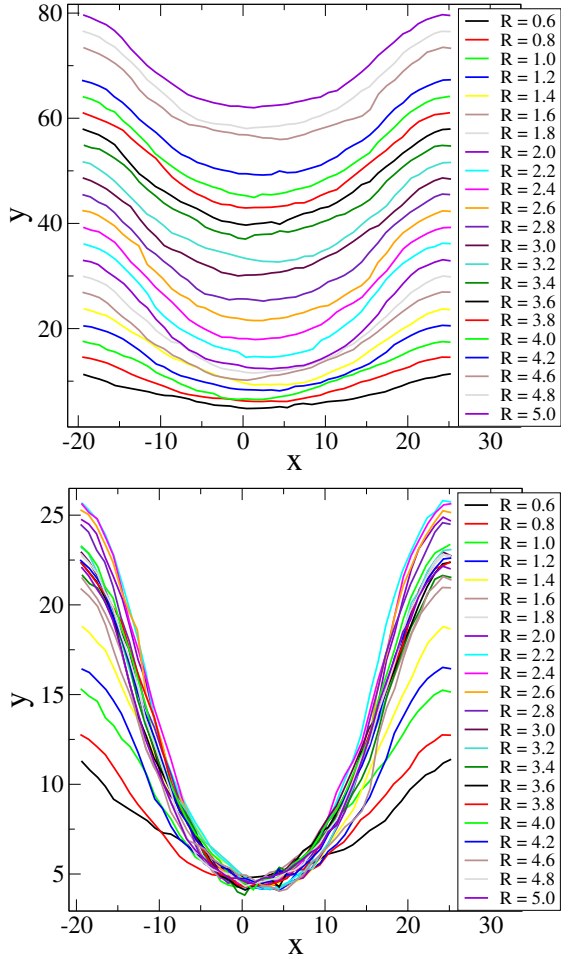


FIG. 4. curvature at a constant strain for different aspect ratio

We wanted to see how the curvature of free boundary

bends under a particular strain for different aspect ratio. We chose a particular temperature $T = 0.20$ and strain rate $\dot{\gamma} = 5 \times 10^{-6}$ and monitored the curvature under a particular strain value $\gamma = 0.553$ for all aspect ratio. In the top panel of Fig.4 we have shown the curvature of the free boundary for different R . It is clear that curvature under a fixed strain is increasing with R . In the bottom panel of Fig.4 we showed the same curvatures but putting all their middle points at the same point. Now it is clear that the curvature is increasing with aspect ratio up to a certain R and then it saturates. Moreover the curvature saturates as it reaches $R = 2.0$ which is exactly the critical aspect ratio at this temperature and strain rate. This observation clearly says that once R reaches the value of corresponding R_C , the curvature of the free boundary immediately starts to saturate and hence to create more surface it generates cavity inside the bulk.

VI. RADIUS OF CURVATURE AS A FUNCTION OF STRAIN FOR DIFFERENT ASPECT RATIO

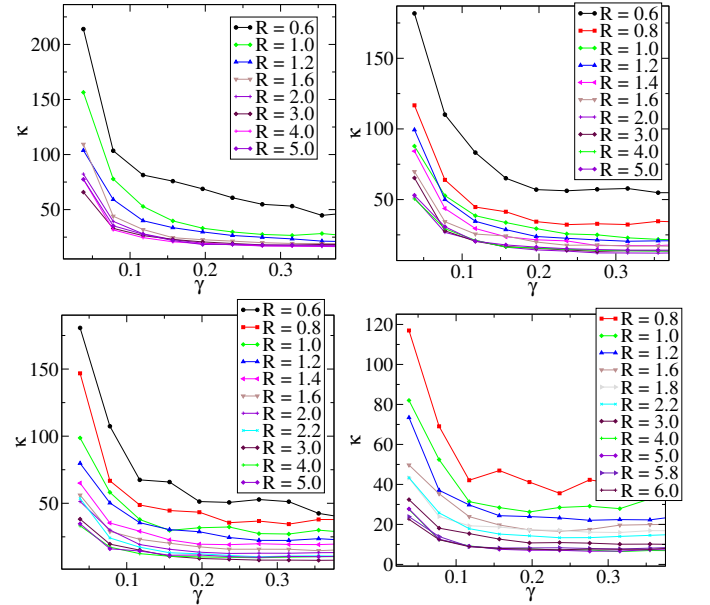


FIG. 5. Radius of curvature as a function of strain at strain rate 5×10^{-6} for $T = 0.15$ (top-left), for $T = 0.20$ (top-right), for $T = 0.25$ (bottom-left), for $T = 0.30$ (bottom-right)

We computed the radius of curvature (\mathcal{K}) as a function of strain for different aspect ratio. In Fig.5 we showed \mathcal{K} as a function of strain at strain rate $\dot{\gamma} = 5 \times 10^{-6}$ for all temperatures. It is clear that for every case \mathcal{K} is decreasing with increasing R as long as R reaches its critical value R_C . Beyond R_C , the radius of curvature saturates and it becomes the same for all aspect ratio greater than R_C . Thus the system can not generate more surface by necking and it leads to creating extra surface

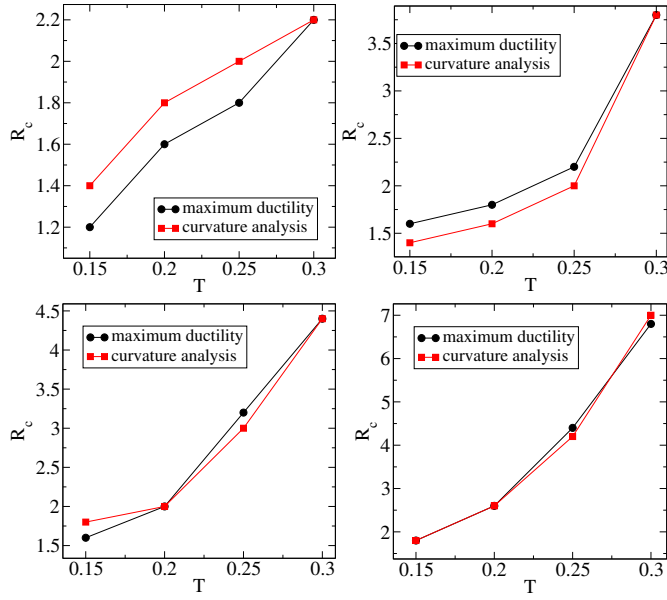


FIG. 6. Comparison of critical aspect ratio between two methods for different temperature T at strain rate $\dot{\gamma} = 5 \times 10^{-5}$ (top-left), 10^{-5} (top-right), 5×10^{-6} (bottom-left), and 10^{-6} (bottom-right)

inside bulk via cavity formation. Since the critical aspect ratio increases with increasing temperature at a constant strain rate, Fig.5 clearly shows the trend of saturation of \mathcal{K} for each temperature.

VII. COMPARISON OF CRITICAL ASPECT RATIO OBTAINED VIA TWO METHODS

Earlier we computed R_C for each temperature and strain rate from the maximum in the ductility Γ vs aspect ratio R curve. Also using the new method of analysing the curvature of the free surface, we computed R_C via eye estimation. We defined R_C to be aspect ratio where the plot of the radius of curvature vs R starts to saturate. We then tried to compare the value of R_C that we computed from these two different methods in Fig.6. This figure shows that our calculated value of R_C from two different methods is very similar. It is even more closely if we choose higher temperature and lower strain rate.

[1] Jeetu S. Babu, Chandana Mondal, Surajit Sengupta, and Smarajit Karmakar, “Excess vibrational density of states

and the brittle to ductile transition in crystalline and amorphous solids,” *Soft Matter* **12**, 1210–1218 (2016).